Correlation of structural and local electronic and magnetic properties of Fe/Cr(001) studied by spin-polarized scanning tunnelling microscopy

2003 J. Phys.: Condens. Matter 15 S2513

(http://iopscience.iop.org/0953-8984/15/34/304)

INSTITUTE OF PHYSICS PUBLISHING JOURNAL OF PHYSICS: CONDENSED MATTER

J. Phys.: Condens. Matter **15** (2003) S2513–S2531 PII: S0953-8984(03)62368-4

Correlation of structural and local electronic and magnetic properties of Fe/Cr(001) studied by spin-polarized scanning tunnelling microscopy

R Ravlić, M Bode and R Wiesendanger

Institute of Applied Physics and Microstructure Research Centre, University of Hamburg, Jungiusstrasse 11, 20355 Hamburg, Germany

Received 16 April 2003, accepted for publication 7 July 2003
Published 15 August 2003
Online at stacks.iop.org/JPhysCM/15/S2513

Abstract

Spin-polarized scanning tunnelling microscopy is applied to study the growth of Fe on Cr(001) as well as the dependence of the electronic and magnetic structure on the Fe coverage. Topographic measurements show an almost perfect layer-by-layer growth except for the coverage range 1.48 ML $< \theta <$ 3 ML, where the second and third layers grow simultaneously. By high-temperature annealing, alloying between the Cr substrate and the Fe film is provoked. Scanning tunnelling spectroscopy (STS) shows that the electronic structure of the resulting c(2×2)-ordered Fe/Cr alloy is governed by a double peaked $\mathrm{d}I/\mathrm{d}U$ spectrum with maxima at $U = -0.3$ and +0.15 V. A time-dependent STS investigation of Fe/Cr(001) reveals that the interface is structurally unstable against alloying. While the spectra are dominated by a single d_{z^2}-like surface state on the day of preparation a double-peak spectrum, indicating the presence of a Fe/Cr alloy, was found one day after preparation. Spin-resolved measurements show that, at small coverage ($\theta \leqslant 0.2$ ML), the Fe islands couple antiferromagnetically to the underlying Cr(001) terraces. The magnetic contrast of the islands and the substrate starts to decrease for $\theta \geqslant 0.22$ ML and completely vanishes at $\theta \geqslant 0.4$ ML. This observation is discussed in terms of a reduction of the Cr Néel temperature due to interdiffusion of Fe into the interface-near region of the Cr substrate. For $\theta \geqslant 3$ ML a weak magnetic contrast reappears which is possibly caused by a spatial variation of the 90° coupling between the Cr substrate and the Fe overlayer.

1. Introduction

Multilayer systems consisting of alternating Cr and Fe layers exhibit an exciting variety of magnetic properties, such as exchange coupling [1], giant magnetoresistance [2] and oscillatory interlayer coupling [3]. As theoretical and experimental investigations showed, the magnetic properties of the multilayer system do not only depend on the Cr film thickness but also correlate

with the intrinsic magnetic structure of Cr and structural properties of the Fe/Cr interface, such as, for example, the occurrence of intermixing.

Clean Cr is an itinerant antiferromagnet being characterized by a transversal spin density wave (t-SDW) below the Néel temperature $T_N = 311$ K which has its origin in the nesting of the Fermi surface. At the spin flip temperature $T_{SF} = 123$ K a transition occurs from a transversal to a longitudinal SDW (l-SDW). In both cases the SDW propagates along the $\{001\}$ directions. It is widely accepted that the exchange coupling at the interface between two semi-infinite Cr and Fe crystals is negative, i.e. Fe and Cr couple antiferromagnetically (AFM). Consequently, a perfect Fe/Cr/Fe trilayer system without any intermixing at the interface should couple ferromagnetically, FM (AFM) for an odd (even) number of Cr atomic layers. While *ab initio* [4] and semiempirical theories [5] support this, experiments using scanning electron microscopy with polarization analysis (SEMPA) [6], Brillouin light scattering (BLS) and magneto-optical Kerr effect (MOKE) [7] revealed that the phase of this short-wavelength oscillation is contrary to the expected behaviour, i.e. an odd (even) number of Cr layers leads to an AFM (FM) coupling of the Fe layers.

One possible explanation was given by Heinrich *et al* [7], who suggested that the π phase shift might be caused by interface alloying. Based on thermodynamical considerations and the difference in the melting point of bulk Fe and Cr it was postulated that interface alloying is restricted to the Cr/Fe interface but does not occur at the Fe/Cr interface. Indeed, scanning tunnelling spectroscopy (STS) measurements by Davies *et al* [8] clearly confirmed the intermixing of Cr grown on a Fe(001) whisker: at the initial stage of Cr deposition on Fe, only 25% of the deposited Cr atoms stay at the surface, while the rest diffuses into the substrate. However, in contradiction to the postulate of reference [7] Choi *et al* [9] revealed that intermixing also occurs if Fe is grown on Cr(001) which—according to reference [7]—would cause another phase shift by π, resulting in a total phase shift of 2π being indistinguishable from the perfect Fe/Cr/Fe interface.

Another important deviation from a perfect interface are steps on the surface. Each terrace of the stepped Cr(001) surface exhibits parallel oriented magnetic moments, but—due to the antiferromagnetism of Cr—adjacent terraces are magnetized antiparallel. This magnetic configuration, the so-called 'topological antiferromagnetism', was predicted by Blügel *et al* [10]. If a Fe film is deposited onto a stepped Cr(001) surface the competition between AFM inter-layer coupling at the Fe/Cr interface and the FM intra-layer coupling in the Fe overlayer must lead to frustration. The resulting domain structure, however, was still unknown.

Our major goal was to directly correlate topographic, electronic and magnetic structure information, as obtained by spin-polarized scanning tunnelling microscopy (SP-STM), to understand the complex magnetic behaviour of Fe/Cr(001). The results show that Fe/Cr(001) is structurally unstable against alloying even at room temperature (RT). While an antiferromagnetic coupling between the Fe islands and the underlying Cr(001) terraces is found at very low Fe coverage ($\theta_{Fe} \leqslant 0.22$ ML) further deposition of Fe leads to a strong decrease of the magnetic contrast until it completely vanishes at $\theta_{Fe} \geqslant 0.4$ ML. Only at $\theta_{Fe} \geqslant 3$ ML does a weak magnetic contrast reappear. This is interpreted in terms of local twisting of the Fe moments which, on average, exhibit a 90° coupling with respect to the Cr substrate but minimize their total energy by the formation of small-angle domain walls at step edge positions of the Cr/Fe interface.

In section 2 of this paper we briefly describe the experimental set-up, tip and sample preparation procedures and the contrast mechanism of SP-STM. After a brief description of the important parameters of the Cr(001) surface in section 3 we will present the STM results of the growth of Fe on Cr(001) in section 4.1. The spin-averaged electronic properties of Fe/Cr(001) dependent on the Fe coverage θ as measured with non-magnetic tips will be

presented in section 4.2. These results unambiguously reveal that an intermixing takes place at the Fe/Cr(001) interface. In section 4.3 we will describe the magnetic behaviour of the Fe/Cr(001) system, starting with an AFM coupling for $\theta \leqslant 0.2$ ML and a transition to a possible 90° coupling for $\theta \sim 3.2$ ML. The results are discussed in section 4.4 and summarized in section 5.

2. Experimental details

All experiments have been carried out in an ultra-high vacuum (UHV) system consisting of a preparation chamber for tip and sample treatment and an analysis chamber for sample surface characterization and combined low-energy electron diffraction (LEED) and Auger electron spectroscopy (AES). The SP-STM measurements were performed at RT with a combined atomic force microscope (AFM) and scanning tunnelling microscope (STM) (maximum scan range 6 μm $\times$ 6 μm) located in a satellite of the analysis chamber. The base pressure in our measurement system is in the low 10^{-11} Torr range.

We used the tip preparation procedure as described in [11]. A polycrystalline W tip is electrochemically etched *ex situ* and cleaned *in vacuo* by a high-temperature flash at $T \geqslant 2200$ K. The STM can be made sensitive to the spin of the tunnelling electron by optional *in vacuo* e^--beam evaporation of a thin Fe film from a carefully degassed Fe rod onto the tip apex. Fe coated tips are preferentially magnetized perpendicular to the tip axis [11, 12] leading to a sensitivity to the in-plane component of the sample surface magnetization. Tunnelling spectra and differential conductivities were measured by adding a modulation voltage $U_{\mathrm{mod}} = 20\ \mathrm{mV_{rms}}$ to the applied sample bias U and recording the $\mathrm{d}I/\mathrm{d}U$ signal by a lock-in technique.

The Cr(001) single crystal was cleaned by overnight Ar^+-ion etching using a sputter gun with a mass filter at elevated temperatures ($T \leqslant 1100$ K) and subsequent annealing for 20–30 min at $T = 1150$ K. Repeating the cleaning cycles for more than two years eventually led to a surface cleanliness which is significantly better than in a previous report [13, 14]; the impurity concentration is less than 3% and is dominated by carbon. All other chemical elements, such as, for example, O, S and N, are below the AES sensitivity limit of $\leqslant$1%.

In order to allow for the comparability with the previous STM study performed by Choi *et al* [9] we have chosen a similar Fe film preparation procedure: RT deposition of Fe at a deposition rate of approximately 0.8–1.0 pseudomorphic monolayers (ML) per minute and postannealing at the temperature $T_{\mathrm{ann}} \approx 480$ K. The Fe deposition rate was calibrated by evaporation and STM analysis of submonolayer Fe films. The indicated total nominal film thickness, which is simply obtained by extrapolation of this deposition rate, may deviate from the apparent coverage, e.g. due to a transition into a non-pseudomorphic growth mode or due to the formation of alloys with a different density. A higher annealing temperature leads to strong diffusion of Fe into the Cr matrix [9]. Even at $T_{\mathrm{ann}} \geqslant 480$ K Choi *et al* [9] reported on the observation of a well-ordered Fe/Cr alloy near step edges and around islands with a compositional ratio of 1:1. In order to possibly avoid this alloy formation we have reduced the annealing time to 4 min. These annealing parameters result in an almost identical island size and shape distribution as reported in [9]. Decreasing the annealing temperature below 480 K or a further reduction of the annealing time leads to relatively rough Fe films. As we will show below, however, intermixing cannot be completely avoided in our set-up because the sample system Fe on Cr(001) is structurally unstable even at RT.

3. The Cr(001) substrate

The constant-current STM image in figure 1(a) shows the topography of a Cr(001) surface. Ten smooth terraces are visible, descending from the lower right to the upper left edge. The

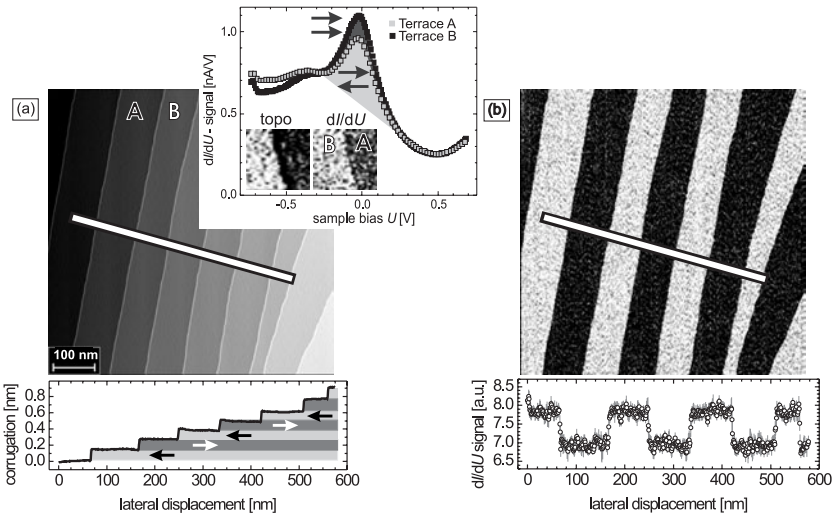

Figure 1. (a) Topography and (b) map of the $\mathrm{d}I/\mathrm{d}U$ signal of the clean Cr(001) surface as measured with a Fe-coated W tip in the constant-current mode. The averaged cross section in the lower panels were drawn along the lines in the images. Neighbouring terraces are always separated by a monatomic step of 1.45 Å height. The inset in (a) shows tunnelling spectra recorded above adjacent terraces A and B being magnetized in opposite directions. As a result of the different relative orientations between tip and sample magnetization the surface state peaks exhibit a distinct intensity variation. The measurement parameters were $U = -150$ mV and $I = 0.7$ nA.

section in the lower panel of figure 1(a) drawn along the line in the image shows that adjacent terraces are separated by monatomic, straight step edges of 1.45 Å height. A distinct peak close to the Fermi level E_F (inset of figure 1(a)) shows up in STS measurements of the Cr(001) surface [13, 14]. This peak was identified as the spectroscopic signature of a d_{z^2}-like surface state which is characteristic for clean bcc(001) surfaces [15]. The cleanliness of the Cr substrate was also corroborated by LEED and AES. The above-mentioned d_{z^2}-like surface state is the minority spin part of an exchange split d-band. It possesses a high spin polarization [13, 16] and is therefore well suited for the spin-polarized scanning tunnelling spectroscopy (SP-STS) carried out by using a magnetic tip. In this case the tunnelling current that flows between the electronically homogeneous Cr(001) sample surface and the tip depends on their relative magnetization directions [17]:

$$I_\mathrm{sp}(\vec{r}, U_0) = I_0[1 + P_\mathrm{s}P_\mathrm{t} \cdot \cos(\vec{M}_\mathrm{s}, \vec{M}_\mathrm{t})], \tag{1}$$

where $I_0 = I_0(\vec{r}, U_0)$ is the non-spin-polarized part of the tunnelling current, $\vec{M}_\mathrm{t}$ and $\vec{M}_\mathrm{s}$ are the magnetization vectors of the tip and the sample, respectively, $P_\mathrm{t} = P_\mathrm{t}(E_\mathrm{F})$ is the spin polarization of the tip at E_F and $P_\mathrm{s} = P_\mathrm{s}(E_\mathrm{F} + eU_0)$ is the spin polarization of the sample at the energy $E_\mathrm{F} + eU_0$.

As mentioned above the magnetic moments of any atomically flat terrace couple parallel but—as a result of the antiferromagnetism of Cr—adjacent terraces are magnetized antiparallel [10]. Since this model implies a close link between the surface topology and the magnetic structure the magnetic state of Cr(001) was called 'topological antiferromagnetism' [10]. Indeed, this prediction was confirmed experimentally by means of SP-STM [13, 14, 16, 18]. The inset in figure 1(a) shows experimental tunnelling spectra which have been measured with a Fe-coated W tip over two neighbouring terraces A and B indicated in figure 1(a). As a result of different relative orientations between the magnetization

of the tip and the sample we observe different peak intensities (cf equation (1)). This intensity variation may be used for mapping the dI/dU signal in the constant-current mode at a suitable bias voltage U simultaneously with the topographic image[1]. For example, figure 1(b) shows a dI/dU map which has been measured simultaneously with the topographic data of figure 1(a) at $U - 150$ mV. Obviously, the dI/dU signal abruptly alternates between two discrete levels when crossing a monatomic step edge separating adjacent Cr(001) terraces, thereby confirming the model of 'topological antiferromagnetism' [10]. Typically, the magnetic variation of the dI/dU signal amounts to 10–12%.

4. Results and discussion

4.1. Structural properties

Figure 2 shows Fe coverage-dependent constant-current images representing the topography of Fe/Cr(001) in the coverage range between 0.05 and 3.2 ML. The data were measured $\leqslant$6 h after preparation. Four different growth ranges can be distinguished: in the first range up to $\theta \leqslant 0.35$ ML we observe the nucleation of isotropic ML islands, preferentially in the middle of Cr(001) terraces, and a roughening of the step edges. The island density successively increases up to 585 ± 55 islands μm^{-2} at $\theta \leqslant 0.35$ ML. While the island shape as well as the island size distribution are in accord with the results of Choi *et al* [9] we do not observe the formation of an ordered Fe/Cr alloy on the terraces around the island rim as reported in [9], probably due to the reduced duration of postannealing from 10 min [9] down to 4 min. We cannot, however, exclude that single Fe adatoms intermix with the Cr substrate, a process which may also be the origin of the step edge roughening.

In the second growth range at 0.4 ML $\leqslant \theta \leqslant$ 1.48 ML we find an almost perfect layer-by-layer growth: after the coalescence of the islands and—though a few small holes remain visible—the completion of the first layer, islands of the second Fe layer nucleate and grow in size. Surprisingly, at a nominal total coverage $\theta = 1.02$ ML the STM data reveal an apparent coverage $\theta = 0.77$ ML, i.e. 0.25 ML lower than expected. A similar observation was made by Choi *et al* [9]: according to the calibration of their Fe evaporation source a coverage of 0.8 ML was expected, but an actual coverage of 0.55 ML was measured by STM and explained by a possible solubility of Fe in the Cr substrate. The deficiency between the nominal total and the apparent coverage was only observed below $\theta \approx 1.2$ ML. Neither on the coalesced first layer nor inside the holes could we detect any hint of an ordered Fe/Cr alloy formation.

Within the error margins the nominal total and the apparent coverage were found to be equal at $\theta > 1.2$ ML, which might point to a coverage-dependent solubility. At $\theta = 1.27$ ML numerous second layer islands can be recognized. The island edges are preferentially oriented along the [100] and [010] directions. Between $\theta = 1.27$ and 1.48 ML the islands of the second layer start to coalesce. As we will show below the surface of the second Fe layer is much smoother than the first, which is a first indication of a thickness-dependent intermixing between Fe and the Cr(001) substrate. This argument is supported by our observation of time-dependent structural changes of Fe films even at RT: while a few small holes are clearly visible in the first layer just upon preparation (cf figure 2 at the corresponding coverage), these holes always disappear within 20 h (not shown here), irrespective of whether the surface is scanned with the STM or not.

The third growth range starts between $\theta = 1.48$ and 1.91 ML. It is characterized by the simultaneous growth of third layer islands and the progressive filling of the holes in the second layer. Again, we found that the surface RMS roughness depends on the local coverage

[1] Details of the contrast mechanism of SP-STM can be found in [14, 18].

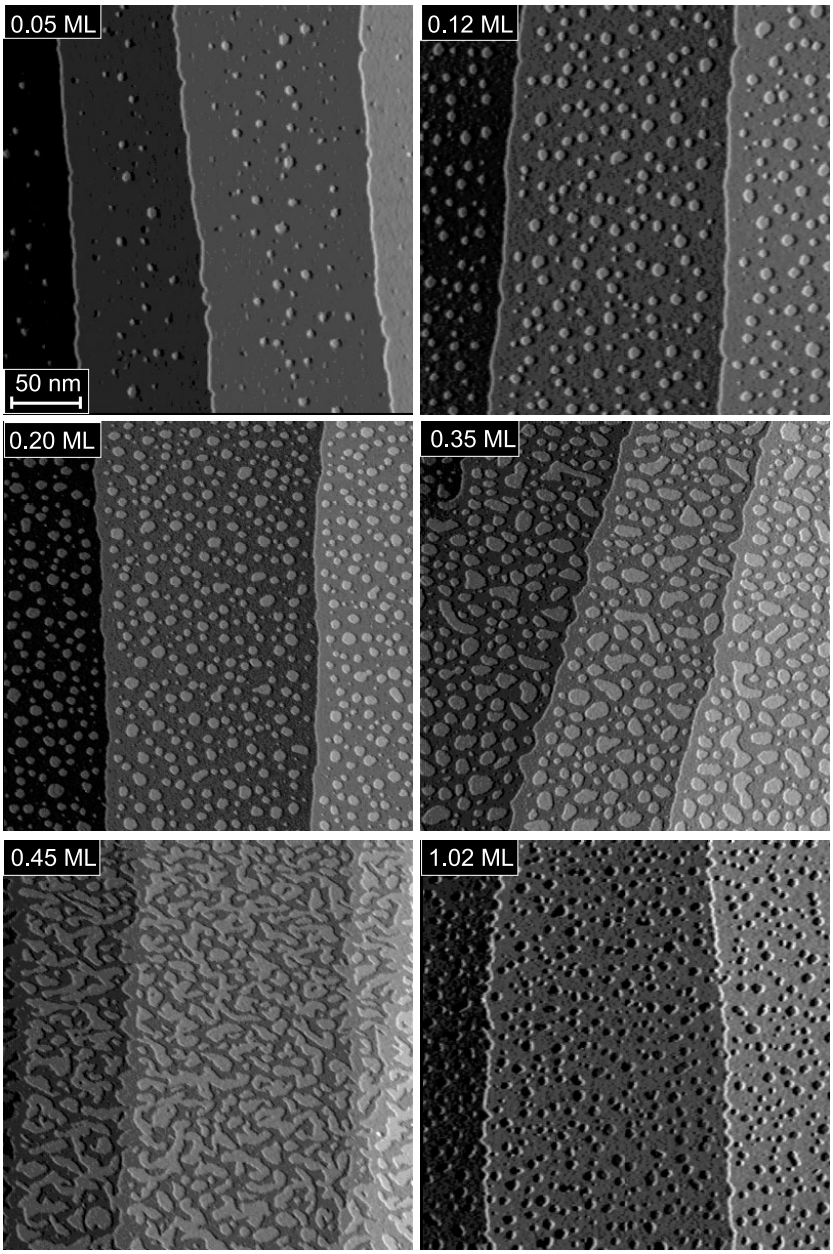

Figure 2. Overview of the growth of Fe on Cr(001). The STM constant-current topographs (image size: 250×250 nm^2) show the topography of Fe/Cr(001) at total nominal coverages between 0.05 up to 3.2 ML. This figure is continued on the next page.

θ_{loc} which—in our interpretation—points to different degrees of intermixing. Figure 3 shows constant-current images of Fe/Cr(001) in the nominal total coverage range between $\theta = 1.02$ and 2.4 ML at higher magnification. At $\theta = 1.02$ ML the first layer exhibits a significant roughness. By comparing regions of different local coverage θ_{loc} it is apparent that the surface roughness is highest for $\theta_{\mathrm{loc}} = 1$ ML and decreases with increasing θ_{loc}. At $\theta = 2.4$ ML

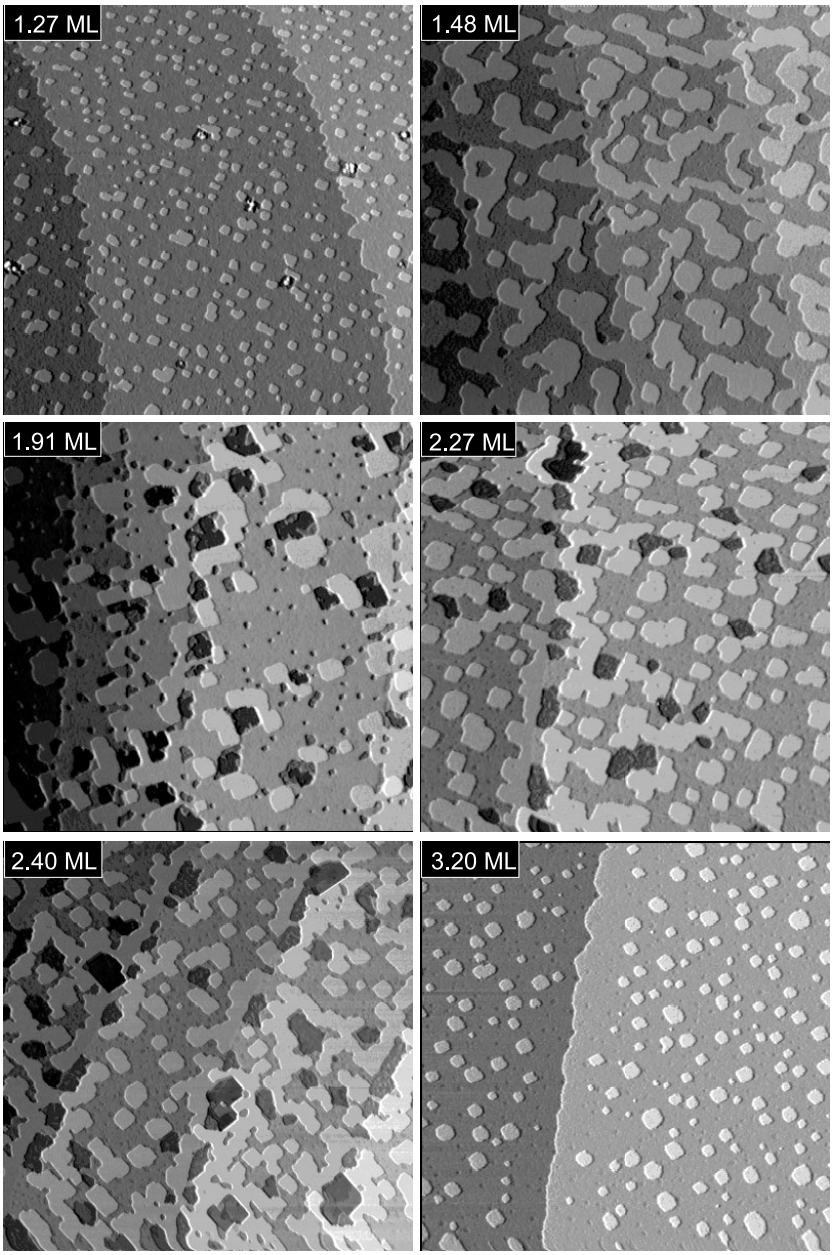

Figure 2. (Continued.)

(bottom right image of figure 3) areas with a reduced apparent height (0.4 Å at $I = 0.5$ nA and $U = -0.2$ V) can be recognized in the second ML. As we will prove later the surface of these areas is the precursor of an ordered Fe/Cr alloy.

In order to estimate the depth and the degree of intermixing between the Fe overlayer and the Cr(001) substrate we have performed coverage-dependent AES before and after annealing of the sample. Hereby, we have taken advantage of the kinetic energy dependence of the

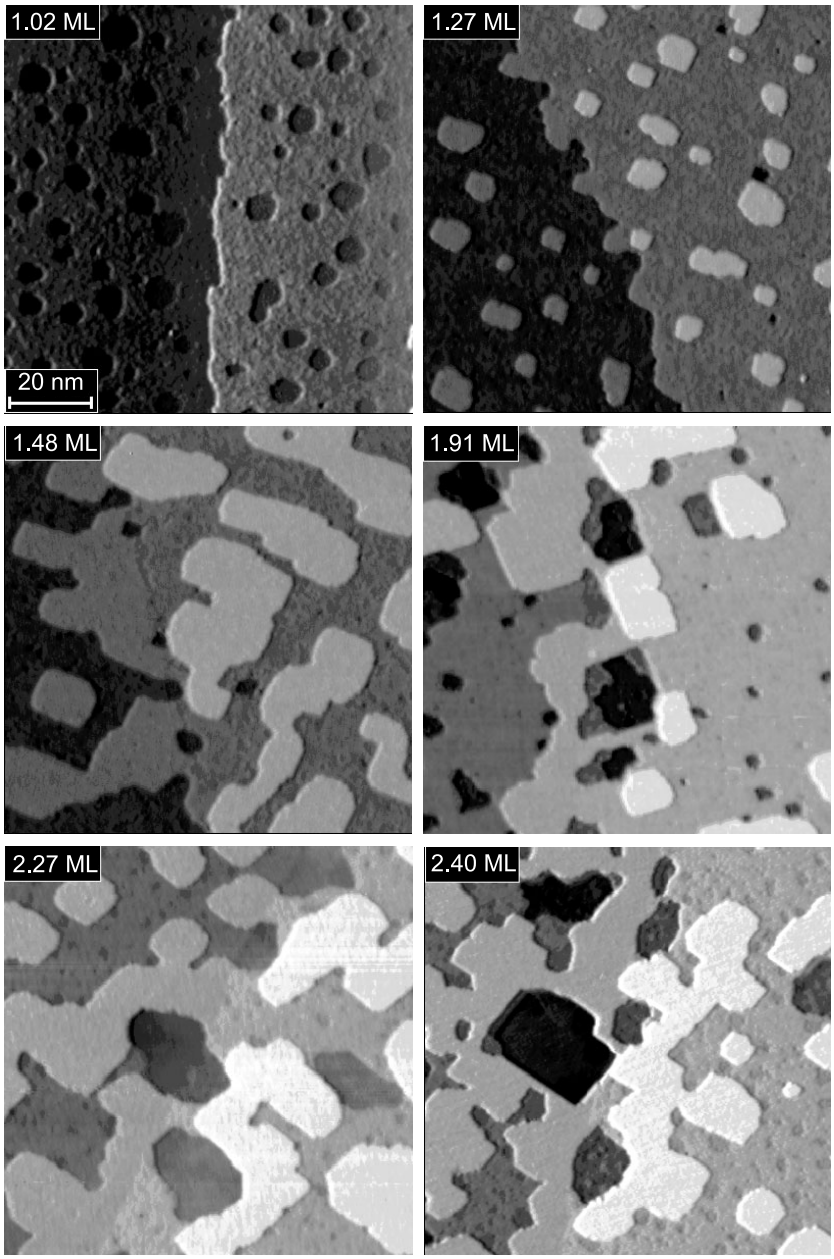

Figure 3. Topographic STM images of Fe/Cr(001) at coverages in the range of $1.02 \leqslant \theta \leqslant 2.4$ ML. The image size is 100×100 nm^2.

electron inelastic mean free path (IMFP) in solids: since the attenuation length of the electrons which stem from MNN transitions λ_{MNN} (kinetic energy $E^{\mathrm{Fe}}_{\mathrm{MNN}} = 47$ eV, $E^{\mathrm{Cr}}_{\mathrm{MNN}} = 36$ eV) is much shorter than λ_{LMM} of electrons from LMM transitions ($E^{\mathrm{Fe}}_{\mathrm{LMM}} = 703$ eV, $E^{\mathrm{Cr}}_{\mathrm{LMM}} = 529$ eV) the AES results should strongly depend on whether or not Cr diffuses to the surface of the overlayer [19].

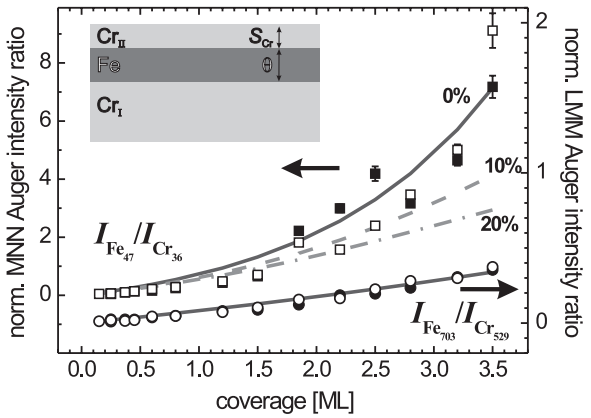

Figure 4. Auger intensities ratios of the LMM (circles) and MNN (squares) lines of Fe (703 and 47 eV, respectively) and Cr (529 and 36 eV, respectively) before (filled) and after (empty) annealing. The plotted curves are generated using the ratio of equations (3) and (2) with $\lambda_{\mathrm{LMM}} = 8$ ML for the $I_{\mathrm{Fe}_{703}}/I_{\mathrm{Cr}_{529}}$ ratio and $\lambda_{\mathrm{MNN}} = 1.5$ ML for the $I_{\mathrm{Fe}_{47}}/I_{\mathrm{Cr}_{36}}$ ratio. The experimental data are fitted best for a surface Cr concentration $S_{\mathrm{Cr}} < 10\%$.

In figure 4 we plotted the intensity ratio of the LMM lines ($I_{\mathrm{Fe}_{703}}/I_{\mathrm{Cr}_{529}}$) (circles) and the intensity ratio of the MNN lines ($I_{\mathrm{Fe}_{47}}/I_{\mathrm{Cr}_{36}}$) (squares) before (full symbols) and after (open symbols) annealing, respectively. The experimental results were fitted by exponential Auger electron creation and attenuation laws under the assumption of a perfect interface without intermixing but with segregation of Cr on top of the Fe layer. Then, the total intensities of Cr, I_{Cr}, and Fe, I_{Fe}, are given by

$$I_{\mathrm{Cr}} = \underbrace{A_{\mathrm{Cr}} \exp\left(-\frac{\theta + S_{\mathrm{Cr}}}{\lambda \cos(\alpha)}\right)}_{\substack{\text{intensity from Cr substrate } (\mathrm{Cr_I}) \\ \text{attenuated through Fe and } \mathrm{Cr_{II}}}} + \underbrace{A_{\mathrm{Cr}}\left[1 - \exp\left(-\frac{S_{\mathrm{Cr}}}{\lambda \cos(\alpha)}\right)\right]}_{\text{intensity from layer } \mathrm{Cr_{II}}} \tag{2}$$

and

$$I_{\mathrm{Fe}} = \underbrace{A_{\mathrm{Fe}}\left[1 - \exp\left(-\frac{\theta}{\lambda \cos(\alpha)}\right)\right]}_{\text{intensity from Fe layer}} \underbrace{\exp\left(-\frac{S_{\mathrm{Cr}}}{\lambda \cos(\alpha)}\right)}_{\text{attenuation through } \mathrm{Cr_{II}}} \tag{3}$$

where A_{Cr} and A_{Fe} are scaling factors which represent the cross sections of the respective Auger transitions, θ is the (homogeneous) Fe coverage of the sample, λ is the IMFP, S_{Cr} is the amount of Cr (in ML) which has diffused onto the film surface and α is the emission angle with respect to the surface normal. We performed our Auger measurements at normal incidence of the primary electron beam, i.e. $\cos\alpha = 1$. With $\lambda_{\mathrm{MNN}} = 1.5$ and $\lambda_{\mathrm{LMM}} = 8$ ML [20] the best agreement between the experimental data points and the ratio of equations (3) and (2) was obtained for $S_{\mathrm{Cr}} < 10\%$. However, on the basis of our AES results a small Cr content in the surface layer cannot be excluded even at high Fe coverage. As we will see later our STS data clearly prove the presence of traces of Fe/Cr alloys at the surface.

Finally, in the fourth growth range at $\theta \geqslant 3$ ML (bottom right panel of figure 2) we observe the recurrence of layer-by-layer growth.

At this point we have to conclude that our aim—the preparation of smooth Fe films on Cr(001) without intermixing—was not accomplished. Although we were able to prevent a vast interdiffusion and the formation of an ordered Fe/Cr alloy by a careful choice of the

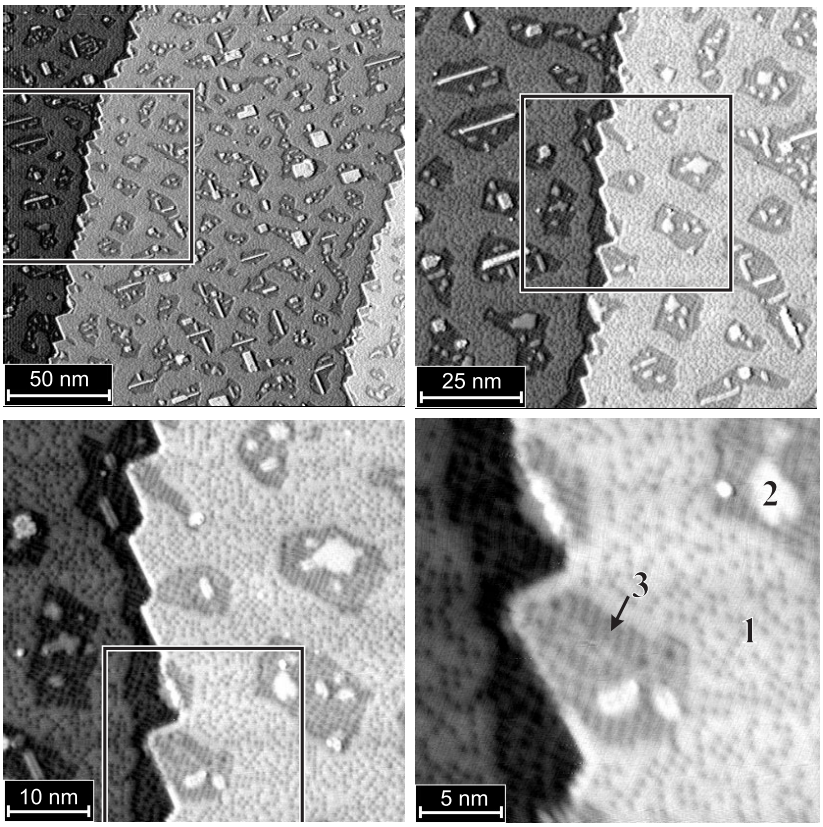

Figure 5. Topographic images of 0.15 ML Fe/Cr(001) after annealing at $T = 630 \pm 100$ K for 4 min. The measurement parameters were $U = -1$ V and $I = 275$ pA. Three different regions can be recognized: (1) terraces with dot-like, approximately 0.2 Å deep indentations, (2) partially needle-shaped islands with an apparent height of 0.6 Å above the terraces and (3) reconstructed areas around the islands and at step edges which appear 0.7 Å deeper than the terraces. The ordered areas (3) around islands and along step edges are identified with a (2×2) Fe/Cr alloy. The dot-like features are probably caused by single Fe atoms in the Cr matrix.

preparation parameters annealing time and temperature, we found indications for a disordered alloy for which the Cr concentration is below the sensitivity limit of our AES apparatus. This interpretation is also supported by investigations of the electronic properties of Fe/Cr(001) which will be presented in the following.

4.2. Electronic properties

The previous section revealed that Fe/Cr(001) cannot be prepared with a perfectly sharp interface. In order to be able to identify the electronic signatures of the c(2×2)-ordered Fe/Cr alloy we have provoked alloying by choosing a higher annealing temperature [9], i.e. at $T = 630$ K for 4 min. The resulting surface topography is shown in four different magnifications in figure 5. Three different regions can be distinguished:

(1) The terraces are decorated with disordered, dot-like, indentations which are 0.5 nm wide (FWHM). At these particular imaging parameters, i.e. $U = -1$ V and $I = 275$ nA, the

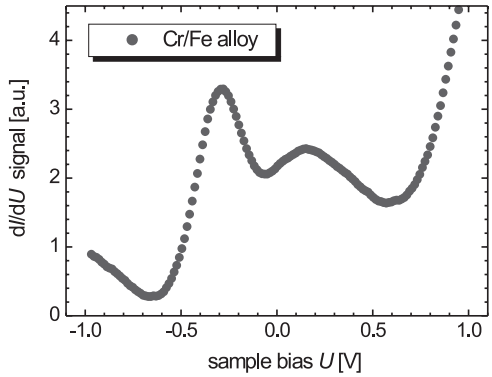

Figure 6. Typical tunnelling spectrum of the c(2 × 2)-ordered Fe/Cr alloy with its characteristic double peak structure.

corrugation of the dots amounts to ≈0.2 Å. These features are probably single Fe atoms which have interdiffused into the Cr(001) surface.

(2) On top of the terraces we find islands which mostly exhibit a needle-like shape. The islands appear approximately 0.6 Å higher than the terraces.

(3) Around the islands a reconstructed area can be recognized which appears to be about 0.7 Å deeper than the terraces.

The latter structures resemble the ordered Fe/Cr alloy which has already been found by Choi *et al* [9]. On these ordered areas we have performed STS measurements. The resulting spectrum is plotted in figure 6. In contrast to clean Cr(001) which exhibits a single peak close to the Fermi level (inset of figure 1), we found a double-peak structure with peaks at $U = -0.3$ and +0.15 V. This spectrum is very similar to the tunnelling spectrum of a single Cr impurity in a Fe(001) whisker surface as described by Davies *et al* [8]. In this case peaks at $U = -0.3$ and +0.2 V were observed. Recent *ab initio* calculations performed by Heinze [21] revealed that the same double peak structure also shows up in a c(2 × 2) ordered Fe/Cr alloy. We speculate that, due to the short screening length of the involved wavefunctions, the electronic structure is dominated by nearest-neighbour atoms. As a consequence of the minor role of next-nearest-neighbour atoms the spectra of single Fe atoms in Cr(001), or single Cr atoms in Fe(001) or an ordered c(2 × 2) Fe/Cr alloy are almost identical.

In the following we have investigated the spin-averaged electronic structure of Fe films on Cr(001) deposited at RT and postannealed at $T_{\mathrm{ann}} \approx 480$ K in dependence of the Fe film thickness and the time elapsed from the moment of sample preparation. Figure 7 shows the tunnelling spectra measured with non-magnetic W tips at total nominal coverages $\theta = 0.2$, 1.02, 1.91 and 2.27 ML (top to bottom panel) on the day of preparation (left column) and approximately 24 h after preparation (right column). In any panel the typical spectra of all local coverages θ_{loc} are shown which appear at the particular nominal coverages. For better visibility different STS curves have been shifted by a constant offset relative to each other.

The top row of figure 7 shows spectra of 0.2 ML Fe/Cr(001). As shown previously (figure 2) the sample consists of the clean substrate and islands with a local coverage $\theta_{\mathrm{loc}} = 1$ ML Fe/Cr(001). Within our measurement accuracy both regions exhibit the same spectrum with a single peak at E_{F} resembling the spectrum of clean Cr(001) as shown in figure 1, which is dominated by a d_{z^2}-like surface state [15]. Since we can exclude on the basis of our AES measurements (figure 4) that the islands appearing on the surface mainly consist of Cr we have to conclude that the spectrum of 1 ML Fe/Cr(001) is almost identical

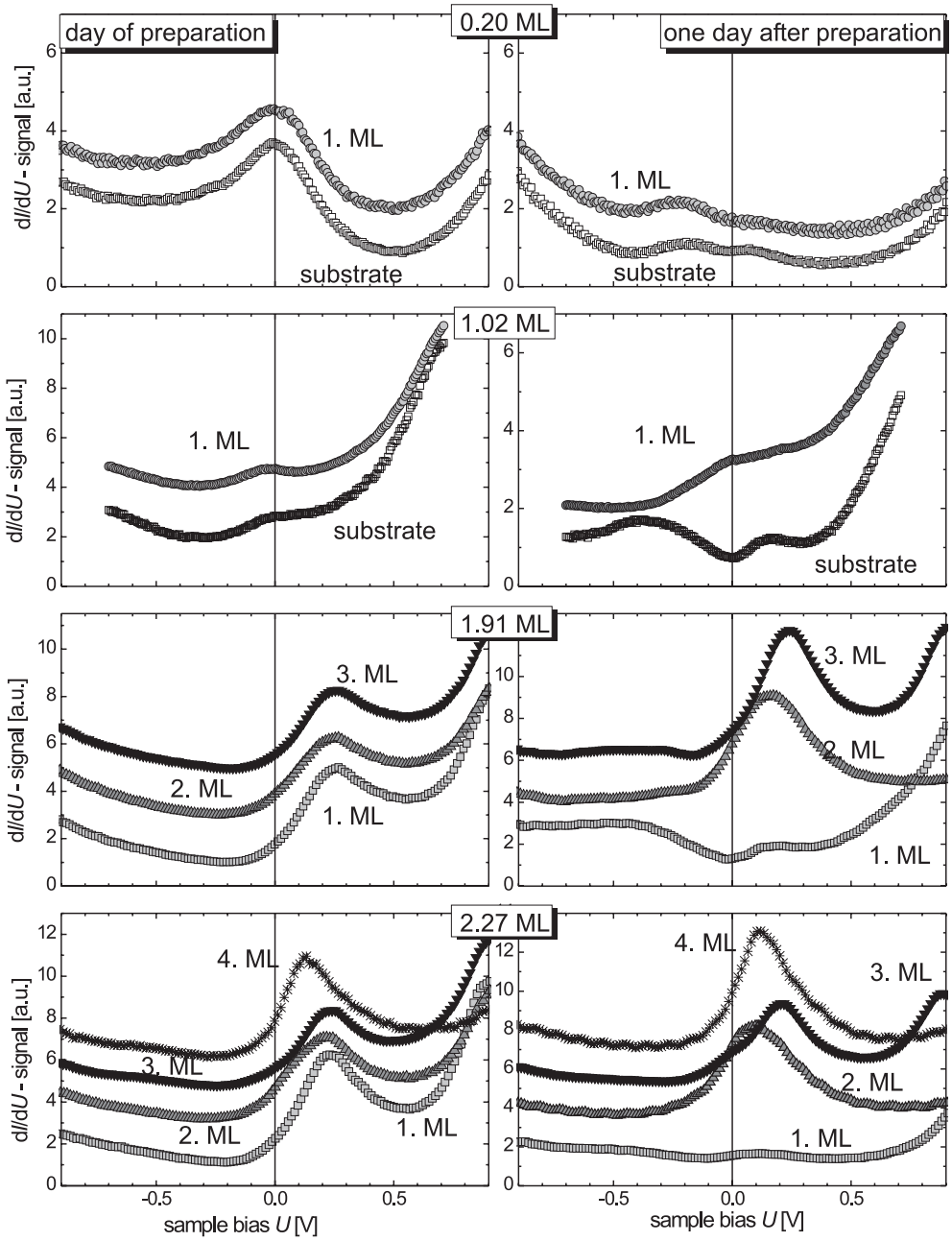

Figure 7. Thickness-dependent electronic structure of Fe films on Cr(001) shortly after (left column) and one day after preparation of the sample (right column) as measured by STS using a non-magnetic W tip. For better visibility different STS curves have been shifted by a constant offset relative to each other. At low coverage ($\theta \leqslant 1.2$ ML) the electronic structure of the substrate and the first ML are similar to that of the clean Cr(001) substrate, i.e. with a single peak at E_{F}. At higher coverage ($\theta \geqslant 1.9$ ML) the peak shifts to $U \approx +0.2$ V. One day after preparation the $\mathrm{d}I/\mathrm{d}U$ spectra of layers closest to the Fe/Cr interface have changed. Now, a double peak structure being characteristic for an ordered Fe/Cr alloy is visible.

to the one for clean Cr(001). One day later (top panel of the right column) the peak at E_F has disappeared. Instead, a weak double peak structure similar to the spectrum in figure 6 is visible. Obviously, the structure of Fe films on Cr(001) is unstable against interdiffusion not only at elevated temperature but—on a timescale of one day—even at RT.

A similar behaviour was observed for 1.02 ML Fe/W(110) (second row of figure 7): although the peak at E_F is weaker than in the previous spectra—an effect which may be caused by different stabilization parameters—it can be clearly recognized for the first ML as well as for the substrate. After one day the spectrum of the substrate exhibits the well-known double peak structure which is even more pronounced than in the case before and clearly indicates the presence of a Fe/Cr alloy. The ML spectrum shows a broad shoulder around E_F.

At a nominal total coverage $\theta = 1.91$ ML the spectra have changed drastically: a single dI/dU peak is found in the empty electronic states at $U \approx +0.25$ V. Though the measured peak position slightly differs from the peak position which has been observed in earlier experiments on clean Fe(001) surfaces, i.e. $U = +0.17$ V, we are confident that it is caused by the d_{z^2}-like surface state of Fe [15]. Therefore, the STS data suggest that the main component of surface layers of this film is Fe. However, STS measurements in the right column, which were performed about one day after film preparation, reveal that the electronic configuration of the first and second layer change with time. Now the first ML shows a clear double peak structure indicating alloy formation. The dI/dU peak of the second layer is shifted to $U \approx +0.1$ V. Only the spectrum of the third layer remained unchanged.

The STS spectra of a sample with a total Fe coverage $\theta = 2.27$ ML are shown in the lowest row of figure 7. Four different local coverages coexist. A similar electronic signature is found in the spectra for $\theta_{loc} = 1$, 2 and 3 ML, i.e. a peak at $U = +0.2$ V. For $\theta_{loc} = 4$ ML the peak position is $U = +0.15$ V. While the spectra of the third and the fourth layer remain unchanged after one day, we observe for the first and second layer a similar behaviour as described before, i.e. a slight shift towards E_F for $\theta_{loc} = 2$ ML and a faint double peak for $\theta_{loc} = 1$ ML.

4.3. Magnetic properties

We have performed magnetically sensitive SP-STS measurements by using Fe-coated W tips. Figure 8 shows typical SP-STS spectra of 0.2 ML Fe/Cr(001) with a topography similar to the respective coverage in figure 2. As indicated by different surface state intensities on adjacent atomically flat terraces the topological antiferromagnetic order of the Cr(001) substrate is maintained in spite of the deposition of Fe onto the sample surface: at E_F the left terrace (empty circles) exhibits a lower dI/dU signal than the right one (empty squares). As mentioned above an antiferromagnetic coupling between Fe and Cr is expected. In fact, the intensities of the dI/dU signal at the surface state peak position as measured above Fe islands (filled circles and squares) are always opposite with respect to those of the underlying Cr(001) terraces.

Based on this knowledge of the spin-resolved electronic structure of the Cr(001) substrate and Fe ML islands the spatial variation of the magnetization direction can be revealed by mapping the spin-resolved dI/dU signal simultaneously with the sample topography. Figure 9 shows a series of topographic images (left) and spin-resolved dI/dU maps (right) at different Fe coverages on Cr(001). Up to a total Fe coverage of $\theta = 0.2$ ML the well-known alternating contrast from adjacent Cr(001) terraces indicates that the topological antiferromagnetic order of the substrate is maintained. Additionally, a clear contrast between islands on different terraces can be recognized: dark islands are found on bright terraces and vice versa. The magnetic contrast amounts up to 10–12%, the same value as found on clean Cr(001). A minute increase of the total Fe coverage, however, leads to a dramatic reduction of the magnetic signal strength. Already at $\theta = 0.22$ ML the contrast between adjacent Cr(001) terraces becomes weaker and

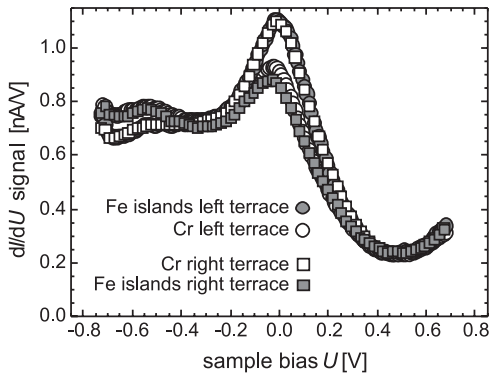

Figure 8. Spin-resolved tunnelling spectra of $\theta \leqslant 0.2$ ML Fe/Cr(001) as measured with a Fe-coated W tip. At the surface state peak position close to E_F ($U = 0$ V) the left Cr terrace (○) exhibits a lower dI/dU signal than the right one (□). The Fe island peaks (●, ■) always behave oppositely with respect to those of the underlying Cr(001) terraces, indicating an antiferromagnetic coupling between Cr and Fe.

the island contrast almost disappears. This trend continues until at $\theta > 0.4$ ML the magnetic contrast of the substrate and the islands completely vanishes. Although we repeatedly tried to achieve magnetic contrast at Fe coverages of 0.4 ML $< \theta <$ 3 ML this was never observed.

However, for $\theta > 3$ ML a weak magnetic contrast reappears. Figure 10 shows the topography (a) and the magnetic dI/dU signal (b) of a 3.2 ML Fe film on Cr(001). While all islands with a local average of 4 ML exhibit the same differential conductivity, a magnetic contrast is found in the dI/dU signal of the closed third layer. Similar to the topological antiferromagnetic order of the uncovered Cr(001) substrate the contrast changes between adjacent terraces. However, this general rule is violated occasionally as can be seen at the left and right sides of figure 10(b): on both sides of the image we find three adjacent terraces which exhibit the same dI/dU signal, an observation which we never made on Cr(001). Furthermore, in many cases the contrast does not change exactly at the position of the surface step edge but slightly left or right from the step edge. We would like to emphasize that the observed contrast was always much lower than for submonolayer films and for the uncovered Cr(001) substrate and never exceeded 1–2%.

4.4. Discussion

Two aspects of the experimental results presented are puzzling, i.e. the absence of magnetic dI/dU contrast in the coverage range 0.4 ML $< \theta <$ 3 ML and the reappearance of a very small magnetic contrast at $\theta > 3$ ML. In our opinion the former is caused by intermixing between the Fe overlayer and the Cr substrate. It is well known that the Néel temperature T_N of Fe_x/Cr_{1-x} alloys strongly depends on the Fe content x [22]: an admixture of only 2% Fe in Cr decreases T_N by 50 K. In other words, even a very small Fe content in the Cr matrix reduces T_N, which amounts to 311 K for pure Cr, below the actual measurement temperature of approximately 290 K. In fact, our STS data have proven that Fe films on Cr(001) are structurally unstable. One day after film preparation the spectra showed a typical double-peak structure which is characteristic for an ordered Fe/Cr alloy. We speculate that, with increasing Fe deposition, the surface-near substrate region accumulates Fe until it becomes paramagnetic at $\theta > 0.4$ ML because $T_N < 290$ K.

The understanding of the magnetic behaviour of the Fe islands is closely related to the underlying substrate. As mentioned above our experimental results reveal that magnetic

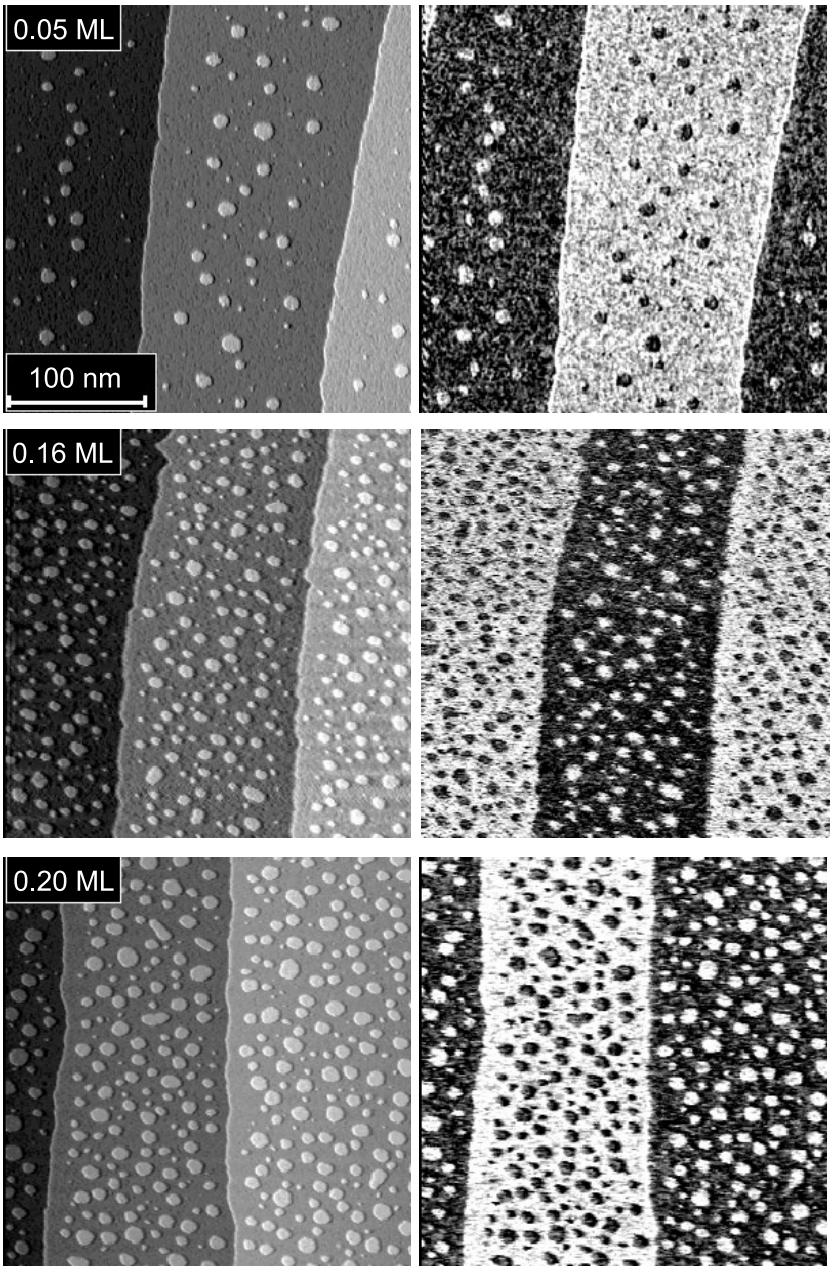

Figure 9. Fe coverage-dependent series of images (250×250 nm^2) showing the topography (left) and the simultaneously recorded spin-resolved $\mathrm{d}I/\mathrm{d}U$ map (right). An AFM coupling of the first Fe layer to the Cr surface is found at $\theta \leqslant 0.2$ ML. An increase of the Fe content leads to a gradually equalization of the $\mathrm{d}I/\mathrm{d}U$ signal of all Fe islands and of the Cr(001) terraces. At $\theta \geqslant 0.33$ ML an almost homogeneous $\mathrm{d}I/\mathrm{d}U$ signal is detected over the whole sample surface. This figure is continued on the next page.

contrast from the Cr substrate remains unchanged up to a Fe coverage of $\theta \leqslant 0.2$ ML. Therefore, the magnetization direction of the Fe islands, which exhibit a diameter of 10–20 nm

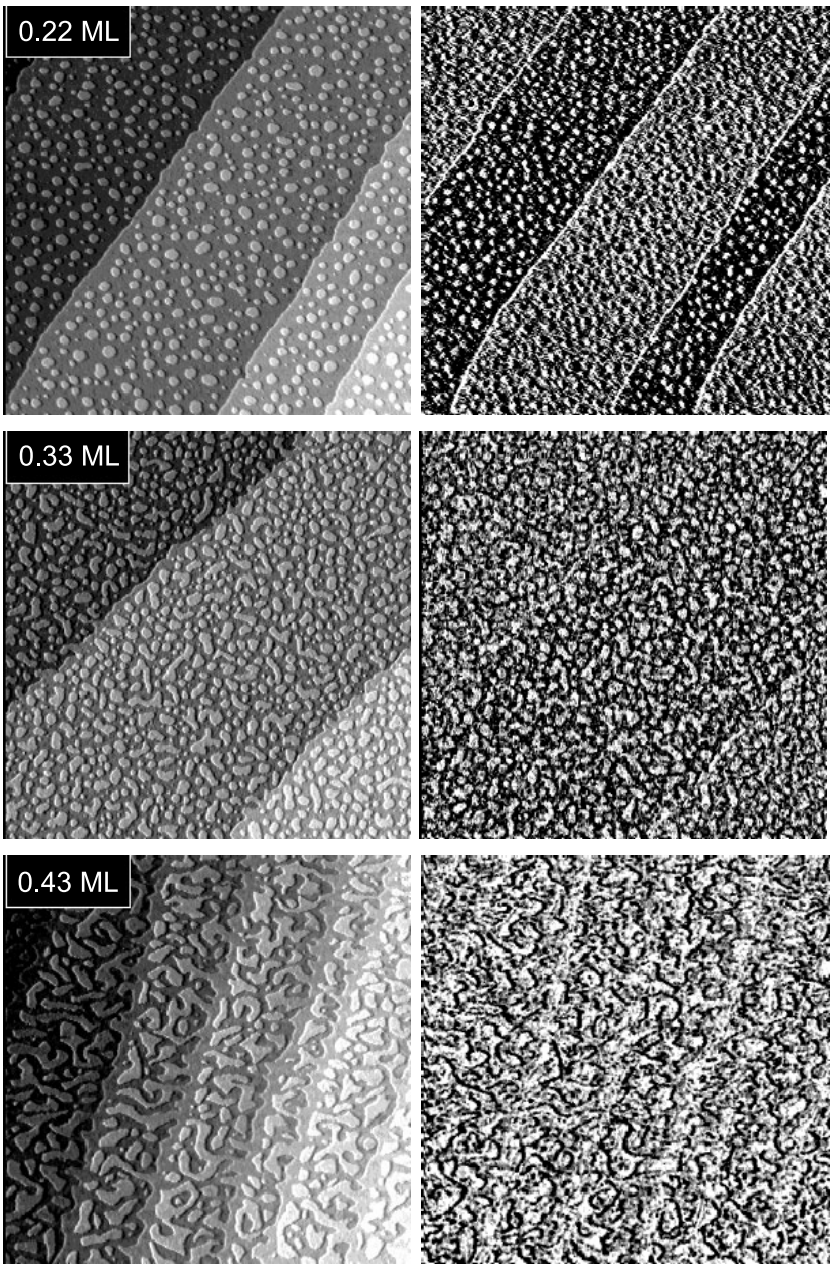

Figure 9. (Continued.)

only and which—due to their small anisotropy barrier—are intrinsically thermally unstable, is governed by the antiferromagnetic exchange coupling to the Cr layer at the interface showing up as opposite contrast between any Cr(001) terrace and the respective Fe adislands (cf figure 9). As a result of an increasing Fe interdiffusion into the interface-near region, however, the Cr magnetic moment at the interface decreases, leading to a gradual decrease of the exchange coupling strength. Eventually, the antiferromagnetic exchange coupling is too small to fix

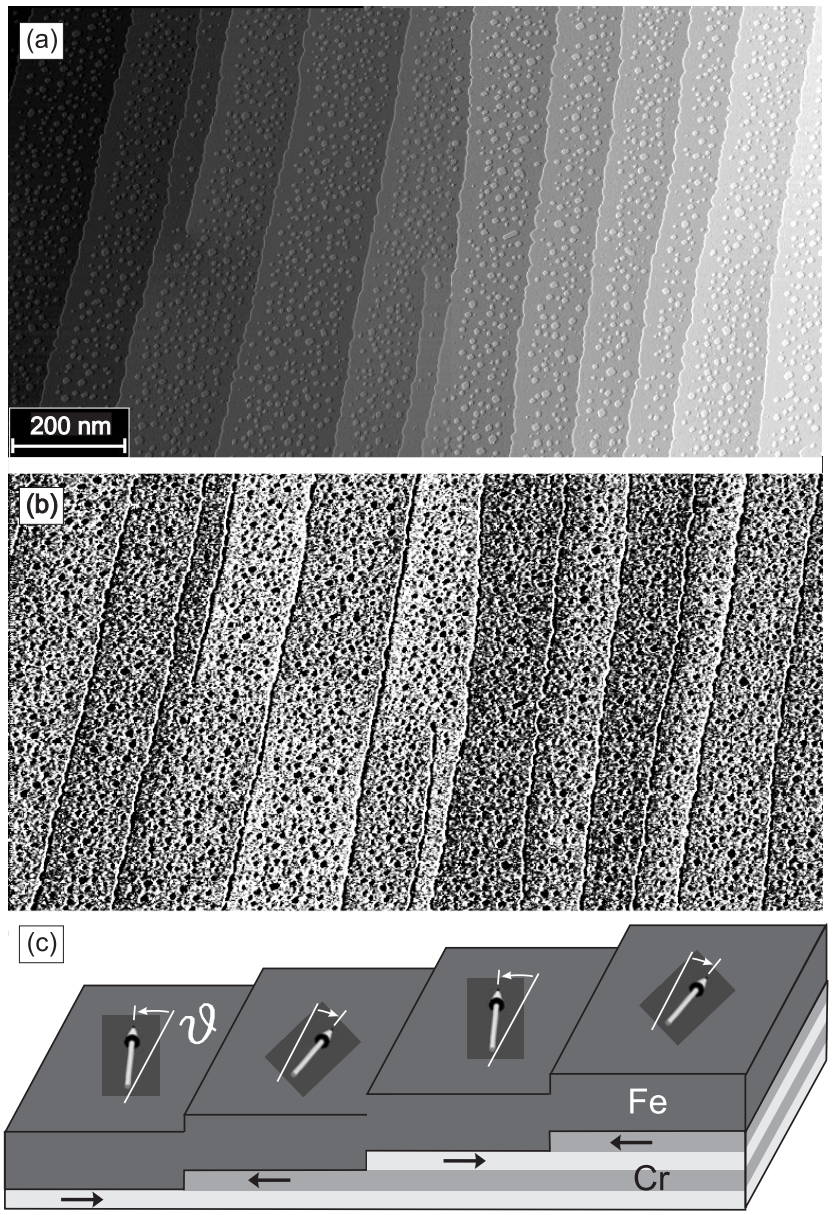

Figure 10. (a) Topography and (b) spin-resolved $\mathrm{d}I/\mathrm{d}U$ map of 3.2 ML Fe/Cr(001). In the central region of (b) a weak magnetic contrast between adjacent terraces can be recognized. (c) This contrast can be explained by a small remaining antiferromagnetic component in the coupling term which describes the exchange between the substrate and the overlayer. This leads to a canting of the Fe magnetization in a direction antiparallel to the magnetization direction of the underlying Cr(001) substrate.

the magnetization against thermal fluctuations and the Fe islands become superparamagnetic, i.e. the island magnetization fluctuates on a much shorter timescale than the scanning frequency of the STM.

Finally, at $\theta \geqslant 3$ ML the Curie temperature T_C exceeds the sample temperature of 300 K and the Fe film becomes ferromagnetic [23]. Now, the ferromagnetic intralayer Fe–Fe interaction, $-J_0 \sum_{ij} \vec{S}_{\mathrm{Fe},i} \cdot \vec{S}_{\mathrm{Fe},j}$, competes with the interfacial Fe–Cr interaction, $J_1 \sum_{ij} \vec{S}_{\mathrm{Cr},i} \cdot \vec{S}_{\mathrm{Fe},j}$. Since the miscut β of our Cr(001) substrate is very low ($\beta \ll 1°$) step-induced anisotropies, which were found to be important at $\beta > 2.5°$ by Escorcia-Aparicio *et al* [24], can be neglected. At a lower miscut angle the competition between the intralayer and the interfacial coupling on the terraced sample on average leads to a 90° coupling [25]. The Fe moments are, however, not perfectly normal with respect to the Cr moments since the Fe–Cr coupling energy $E_1 \approx J_1 \vartheta W/a$, with W being the terrace width and a the lattice constant, can be lowered by twisting the Fe moments within the film plane by an angle ϑ into the direction antiparallel to the underlying Cr terrace [24]. Of course, on adjacent terraces the twisting occurs in opposite directions. This situation is schematically represented in figure 10(c). Under the assumption that the resulting ϑ-degree domain wall ranges over the full terrace width W the wall energy is given by $E_0 = J_0 \vartheta^2 d_{\mathrm{Fe}}/W$, where d is the Fe film thickness [24]. Since the actual terrace width exceeds 100 nm while the exchange length of bulk Fe only amounts to $L = 21$ nm we can replace W by L. By minimization of the total energy Escorcia-Aparicio *et al* [24] found $\vartheta \approx J_1 W^2/(2J_0 ad)$. With $J_0/k_B = 375$ K and $J_1/k_B = -40$ K [26] we get $\vartheta = 18°$. On clean Cr(001)—a material with comparable electronic properties—a 180° wall causes a $\mathrm{d}I/\mathrm{d}U$ signal variation of 10%. Since the contrast scales with the projection of the sample onto the tip magnetization we shall expect a contrast of 3% for a 2ϑ (36°) domain wall. This result is in fair agreement with the magnetic contrast strength of the $\mathrm{d}I/\mathrm{d}U$ signal of 2% observed in figure 10(b).

A closer comparison between figures 10(a) and (b) reveals that the contrast changes do not always coincide with surface step edges. This may be caused by surface and interface step edge positions that do not match but are slightly shifted with respect to each other, leading to a lateral variation of the local Fe coverage. As a result we may observe a surface step edge that does not lead to a change of the magnetic contrast since the magnetization direction of the underlying (atomically flat) Cr substrate remains the same. In order to prove this hypothesis an experimental technique is needed which—in contrast to SP-STM—is not exclusively sensitive to the topmost surface layer but also yields information from buried layers and interfaces.

5. Summary and outlook

In this work we have described STM/STS results on the correlation between structural, local electronic and local magnetic properties of Fe films grown on a Cr(001) substrate up to a coverage of a few monatomic layers. Our results reveal an almost perfect layer-by-layer growth for $\theta \leqslant 1.48$ ML and for $\theta \geqslant 3$ ML. In the intermediate coverage range (1.48 ML $< \theta <$ 3 ML) the simultaneous growth of second and third ML islands is observed. The Fe films on Cr(001) are unstable against intermixing even at RT. This is shown by time-dependent topological and electronic structure investigations. Magnetically sensitive SP-STS measurements show that, at $\theta \leqslant 0.2$ ML, the Fe islands couple antiferromagnetically to the underlying Cr(001) terraces. The magnetic contrast decreases for $\theta \geqslant 0.22$ ML and vanishes at $\theta \geqslant 0.4$ ML Fe/Cr(001). This observation may be caused by a decreasing exchange coupling between the Fe islands and the Cr substrate due to a diffusion of Fe into the interface near Cr which leads to a reduction of the Cr Néel temperature below the measurement temperature of 300 K. This hypothesis may be checked by future variable temperature SP-STS experiments. We found that a weak magnetic contrast reappears for $\theta \geqslant 3$ ML which is possibly caused by a spatial variation of the 90° coupling between the Cr substrate and the Fe overlayer.

Acknowledgments

Financial support from the DFG (grant no WI1277 and Graduiertenkolleg 'Physik nanostrukturierter Festkörper') is gratefully acknowledged. We thank W Kuch (MPI Halle) for helpful discussions.

References

[1] Grünberg P, Schreiber R, Pang Y, Brodsky M B and Sowers H 1986 *Phys. Rev. Lett.* **59** 2442
[2] Baibich M N, Broto J M, Fert A, Dau F N V, Petroff F, Eitenne P, Creuzet G, Friederich A and Chazelas J 1988 *Phys. Rev. Lett.* **61** 2472
[3] Parkin S S P, More N and Roche K P 1990 *Phys. Rev. Lett.* **64** 2304
[4] Herman F, Sticht J and Schilfgaarde M V 1999 *J. Appl. Phys.* **69** 4783
[5] Vega A, Rubio A, Balbas L C, Dorantes-Davila J, Bouarab S, Demangeat C, Mokrani A and Dreyssé H 1991 *J. Appl. Phys.* **69** 4544
[6] Unguris J, Celotta R J and Pierce D T 1991 *Phys. Rev. Lett.* **69** 1125
[7] Heinrich B, Cochran J F, Monchesky T and Urban R 1999 *Phys. Rev.* B **59** 14520
[8] Davies A, Stroscio J A, Pierce D T and Celotta R J 1996 *Phys. Rev. Lett.* **76** 4175
[9] Choi Y J, Jeong I C, Park J-Y, Kahng S-J, Lee J and Kuk Y 1999 *Phys. Rev.* B **59** 10918
[10] Blügel S, Pescia D and Dederichs P H 1989 *Phys. Rev.* B **39** 1392
[11] Bode M, Pietzsch O, Kubetzka A and Wiesendanger R 2001 *J. Electron Spectrosc. Relat. Phenom.* **114–116** 1055
[12] Bode M, Pietzsch O, Kubetzka A, Heinze S and Wiesendanger R 2001 *Phys. Rev. Lett.* **86** 2142
[13] Kleiber M, Bode M, Ravlić R and Wiesendanger R 2000 *Phys. Rev. Lett.* **85** 4606
[14] Kleiber M, Bode M, Ravlić R, Tezuka N and Wiesendanger R 2002 *J. Magn. Magn. Mater.* **240** 64
[15] Stroscio J A, Pierce D T, Davies A, Celotta R J and Weinert M 1995 *Phys. Rev. Lett.* **75** 2960
[16] Wiesendanger R, Güntherodt H J, Güntherodt G, Gambino R J and Ruf R 1990 *Phys. Rev. Lett.* **65** 247
[17] Slonczewski J C 1989 *Phys. Rev.* B **39** 6995
[18] Ravlić R, Bode M, Kubetzka A and Wiesendanger R 2003 *Phys. Rev.* B **67** 174411
[19] Schmid A, Atlan D, Itoh H, Heinrich B, Ichinokawa T and Kirschner J 1993 *Phys. Rev.* B **48** 2855
[20] Seah M P and Dench W A 1979 *Surf. Interface Anal.* **1** 2
[21] Heinze S 2002 Private communication
[22] Fawcett E, Alberts H L, Galkin V Y, Noakes D R and Yakhmi J V 1994 *Rev. Mod. Phys.* **66** 25
[23] Guo W, Shi L P and Lin D L 2000 *Phys. Rev.* B **62** 14259
[24] Escorcia-Aparicio E J, Choi H J, Ling W L, Kawakami R K and Qiu Z Q 1998 *Phys. Rev. Lett.* **81** 2144
[25] Slonczewski J C 1991 *Phys. Rev. Lett.* **67** 3172
[26] Bödeker P, Hucht A, Schreyer A, Borchers J, Güthoff F and Zabel H 1998 *Phys. Rev. Lett.* **81** 914